Magnetism and transport in transparent high-mobility $BaSnO_3$ films doped with La, Pr, Nd, and Gd

Urusa S. Alaan,[1,2,*] Franklin J. Wong,[3] Jeffrey J. Ditto,[4,5] Alexander W. Robertson,[4] Emily Lindgren,[1,2] Abhinav Prakash,[6] Greg Haugstad,[7] Padraic Shafer,[8] Alpha T. N'Diaye,[8] David Johnson,[5] Elke Arenholz,[8,9] Bharat Jalan,[6] Nigel D. Browning,[4,10] and Yuri Suzuki[2,11]

[1]*Department of Materials Science and Engineering, Stanford University, Stanford, California 94305, USA*
[2]*Geballe Laboratory for Advanced Materials, Stanford University, Stanford, California 94305, USA*
[3]*Department of Materials Science and Engineering, University of California, Berkeley, Berkeley, California 94720, USA*
[4]*Physical and Computational Sciences Directorate, Pacific Northwest National Laboratory, Richland, Washington 99354, USA*
[5]*Department of Chemistry and Biochemistry, University of Oregon, Eugene, Oregon 97403, USA*
[6]*Department of Chemical Engineering and Materials Science, University of Minnesota, Minneapolis, Minnesota 55455, USA*
[7]*Characterization Facility, University of Minnesota, Minneapolis, Minnesota 55455, USA*
[8]*Advanced Light Source, Lawrence Berkeley National Laboratory, Berkeley, California 94720, USA*
[9]*Cornell High Energy Synchrotron Source, Cornell University, Ithaca, New York 14853, USA*
[10]*School of Engineering and School of Physical Sciences, University of Liverpool, Liverpool L69 3BX, United Kingdom*
[11]*Department of Applied Physics, Stanford University, Stanford, California 94305, USA*

(Received 10 July 2019; revised manuscript received 12 October 2019; published 9 December 2019)

We have explored the effect of magnetic rare-earth dopants substitutionally incorporated on the Ba sites of $BaSnO_3$ in terms of electronic transport, magnetism, and optical properties. We show that for $Ba_{0.92}R_{0.08}SnO_3$ thin films (where R = La, Pr, Nd, Gd), there is a linear increase of mobility with carrier concentration across all doping schemes. La-doped films have the highest mobilities, followed by Pr- and Nd-doped films. Gd-doped samples have the largest ionic size mismatch with the Ba site and correspondingly the lowest carrier concentrations and electron mobilities. However, crystallinity does not appear to be a strong predictor of transport phenomena; our results suggest that point defects more than grain boundaries are key ingredients in tuning the conduction of $BaSnO_3$ films grown by pulsed laser deposition. Pronounced, nonhysteretic x-ray magnetic dichroism signals are observed for Pr-, Nd-, and Gd-doped samples, indicating paramagnetism. Finally, we probe the optical constants for each of the $BaSnO_3$ doping schemes and note that there is little change in the transmittance across all samples. Together these results shed light on conduction mechanisms in $BaSnO_3$ doped with rare-earth cations.

DOI: 10.1103/PhysRevMaterials.3.124402

I. INTRODUCTION

A significant challenge in the field of oxide electronics over the past several decades has been the search for materials with high room-temperature carrier mobilities that can also be epitaxially integrated with complex oxides [1–4]. Several strongly correlated complex oxides configure themselves in the perovskite (ABO_3) crystal structure [3]. Until recently, La-doped $SrTiO_3$ was among the highest mobility perovskite-structure oxides with $\mu \sim 53\,200$ cm^2/V s at 2 K, but dropping to only $\sim$7 cm^2/V s at 300 K [2,5]. For this reason, the demonstration by Luo *et al.* that La-doped $BaSnO_3$ could have room-temperature mobilities higher than 100 cm^2/V s in bulk crystals attracted significant attention [6]. Shortly thereafter, Kim *et al.* synthesized La-doped $BaSnO_3$ with room-temperature mobilities exceeding 300 cm^2/V s in bulk crystals; together these studies were a breakthrough in the field of oxide electronics [7–9]. Thin films of La-doped $BaSnO_3$ have achieved $\mu \sim 180$ cm^2/V s by molecular beam epitaxy (MBE) on lattice-matched (110) $DyScO_3$ substrates and $\mu \sim 100$ cm^2/V s by pulsed laser deposition (PLD) when $BaSnO_3$ was grown homoepitaxially [9–12]. In addition to having a perovskite crystal structure and high carrier mobilities, La-doped $BaSnO_3$ is both transparent and colorless in the visible wavelength regime, even when it is degenerately doped [6,13].

The discovery of this new class of transparent conducting oxides unlocks new opportunities for applications ranging from thin-film transistor-based displays to oxide photovoltaic systems. In addition, spintronic devices that require interfaces between metallic or semiconducting films and perovskite ferromagnets would benefit from the availability of lattice-matched materials. Moreover, the combination of three functional properties—low resistivity and high carrier mobility, optical transparency, and a magnetic moment—together in a single material would help to enable the realization of an all-oxide spintronics platform for low-power, low-energy-consumption devices.

There have been several efforts toward doping transparent conducting oxides (TCOs) to make them ferromagnetic, with varying degrees of success. The focus of nearly all studies on magnetically doping $BaSnO_3$ has been on the incorporation of transition metals such as Mn, Fe, and Co onto the $BaSnO_3$ lattice with substitution occurring on the Sn^{4+} site [14–20].

*usalaan@gmail.com

These compounds have generally exhibited ferromagnetic insulating behavior and are opaque in the visible wavelength range. If the ferromagnetism is intrinsic, it is hypothesized to result from an "F-center exchange" mechanism that relies on oxygen vacancies that trap electrons and cause local ferromagnetic ordering [21]. However, the need for charge carriers to be localized and strongly coupled to defect sites impedes their conduction. Efforts to co-dope $BaSnO_3$ with two transition metals on the Sn site to add both conduction and a magnetic moment have also resulted in insulating materials [22]. Because electrical transport is governed by the conduction band with Sn 5*s* character, disruption of these *B*-sites causes both a loss of electrical conductivity as well as the occurrence of optical absorption in the visible regime. Furthermore, ferromagnetism itself is not reproducible across different studies, and d^0 magnetization is difficult to decouple from dilute transition-metal doping, intrinsic contamination (e.g., phase segregation) and extrinsic contamination (e.g., magnetic dust) [19,20].

For these reasons, a more attractive route to designing a transparent, ferromagnetic semiconductor is through exploitation of the perovskite *A*-site, a degree of freedom in $BaSnO_3$ that is not accessible in binary TCO systems [19,23]. Previously we demonstrated *A*-site doping of $BaSnO_3$ films with 4% Gd [23]. These films exhibit optical transparency and electron mobilities of 30 $cm^2/V\,s$ at room temperature. While these Gd-doped films showed a strong paramagnetic signal at low temperatures, the magnetization was not hysteretic. The absence of ferromagnetism is likely due to two factors: an insufficient doping level and a strongly localized wave function for Gd. In this study, we address both issues through dopant concentration and selection, respectively.

Long-range ferromagnetic order in ABO_3 perovskites is generally mediated by B-O-B indirect exchange interactions as A-O-A interactions are much weaker. Thus, if rare-earth doped $BaSnO_3$ were ferromagnetic, the coupling would be indirect because of the large distance between the magnetic impurities with low doping levels, as well as the localized nature of the $4f$ wave function. For this reason, Ruderman-Kittel-Kasuya-Yosida (RKKY) interactions may play a role in a system with a sufficient concentration of delocalized electrons, more so than oxygen-mediated exchange. In the $4f$ block, localization of the wave function increases with atomic number Z, so it could be advantageous to choose lower Z lanthanide dopants such as Pr and Nd. However, these also have fewer unpaired electrons than Gd, resulting in a lower moment overall. There is therefore a tradeoff in rare-earth dopant selection. Recently, McCalla *et al.* have demonstrated Pr- and Nd-doping of up to 0.5% in $BaSnO_3$ single crystals; these bulk samples showed good transport properties as well as paramagnetic behavior [24]. There have also been recent studies of 7% Nd-doped $BaSnO_3$ films with metallic conduction but no report on magnetic response [25].

Toward developing optical and magnetoelectric functionality in single material, we have doped $BaSnO_3$ (BSO) films with 8% Pr, Nd, and Gd on the Ba sites. We have also synthesized 8% La-doped $BaSnO_3$ films as a control. This study shows the impact of dopant ionic radii on structure and transport properties, and it also demonstrates that $BaSnO_3$ films can remain transparent at high concentrations of rare-earth doping. All films showed high electron mobilities and degenerate doping. Moreover, up to 8% Pr, Nd, and Gd doping of $BaSnO_3$ gives rise to strong paramagnetic responses, although no long-range order of dopant moments is observed.

II. EXPERIMENT

Thin films were grown by pulsed laser deposition (PLD) from sintered ceramic targets of $Ba_{0.92}La_{0.08}SnO_3$ (BLSO), $Ba_{0.92}Pr_{0.08}SnO_3$ (BPSO), $Ba_{0.92}Nd_{0.08}SnO_3$ (BNSO), and $Ba_{0.92}Gd_{0.08}SnO_3$ (BGSO). All targets were synthesized by Toshima Manufacturing Company. An excimer laser (KrF, $\lambda = 248$ nm) was used to ablate the rotating targets with an energy density of $\sim 1.4\ J/cm^2$. Growth of conducting samples was performed at 100 mTorr O_2 and 750 °C with a 2.5-in. distance separating the target from the (001) oriented single crystal $SrTiO_3$ substrates. Growth in a poorer oxygen atmosphere (3.5×10^{-3} Torr) resulted in insulating samples, albeit with similar crystalline quality to the conducting samples. The electronic properties of the samples were also particularly sensitive to the target-heater distance, with larger distances leading to more insulating films. The $SrTiO_3$ substrates were etched in hydrofluoric acid and annealed at 1000 °C, yielding TiO_2-terminated surfaces. While the termination itself was not important in this study, this etching procedure was conducted for the purpose of removing surface contaminants. Care was taken so that the samples were never handled with metal tweezers or any other ferromagnetic object.

Magnetometry was conducted in a Quantum Design Evercool Magnetic Property Measurement System (MPMS) with the reciprocating sample option (RSO). Samples were field-cooled in $H = +7$ T to 4.5 K before beginning measurements, and the orientation of the field was always in the plane of the sample along the {100} type directions. A Quantum Design Physical Property Measurement System (PPMS) was used for current-sourced electrical transport experiments. Thin-film samples were bonded with Al wire in a four-point van der Pauw geometry for Hall effect measurements between ± 7 T. Optical properties and thicknesses were found from measurements on a J. A. Woollam M2000 spectroscopic ellipsometer with the depolarization option, and models were constructed using the corresponding WVASE32 software. Thicknesses were also deduced from Rutherford backscattering spectrometry (RBS), ellipsometry, and x-ray reflectivity (XRR) for thinner samples. RBS was performed on a MAS 1700 pelletron tandem ion accelerator equipped with an analysis endstation, and RBS data were analyzed with SIMNRA software. A Panalytical X'Pert diffractometer with a Cu $K\alpha 1$ source was used for x-ray diffraction (XRD) and XRR measurements. Surface morphology was studied by atomic-force microscopy (AFM) using a Digital Instruments Dimension 3100 tool. X-ray absorption (XAS) and x-ray magnetic circular dichroism (XMCD) measurements were conducted at the Advanced Light Source (ALS) using Beamlines 4.0.2 and 6.3.1 in total electron yield mode (TEY) at a 30 °C grazing angle of incidence.

III. RESULTS

A. Structure

All the doped films grown at 750 °C, 100 mTorr O_2, and 2.5 in. target-to-substrate distance show similar structural

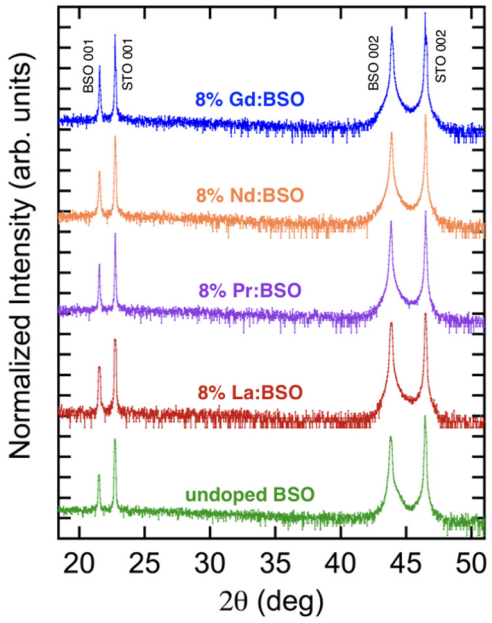

FIG. 1. X-ray diffraction spectra of 8% Gd-, Nd-, Pr-, and La-doped $BaSnO_3$ films as well as undoped $BaSnO_3$ films. The out-of-plane lattice parameter decreases toward the bulk value as the Ba-site dopant decreases in ionic radius. The spectra are normalized by substrate intensity and shifted for clarity.

properties. Representative θ-2θ spectra as measured by x-ray diffraction are given in Fig. 1. Despite the large lattice mismatch of the films ($a = 4.117$ Å for bulk BSO) on the underlying (001) $SrTiO_3$ substrates ($a = 3.901$ Å), they are epitaxial and of good structural quality [3,11]. When grown thin enough, they show Kiessig fringes in x-ray reflectivity and Laue oscillations around the 002 Bragg reflection [26]. The films were highly crystalline with a typical rocking curve full width at half-maximum of $\Delta\omega_{002} \sim 0.04\,^{\circ}$C. Table I gives the out-of-plane (OOP) lattice parameters (a_{OOP}) as well as rocking curve full width at half-maximum ($\Delta\omega_{002}$) measured around the 002 Bragg reflections for films with thicknesses between 270 and 300 nm. Lattice constants for all doped films are shown in the supplemental material [27].

It is evident that there is quite a large mismatch between the rare-earth cation sizes and the host barium site; for Gd^{3+} the size difference is over 20%. And yet for all rare-earth doping cases, including gadolinium, there is a slight *increase* of the lattice parameters from that of undoped $BaSnO_3$ bulk ($a = 4.117$ Å) [31] as shown in Table I. It appears that the presence of charged defects serves to expand the lattice due to Coulombic repulsion effects. This is also consistent with the results on La-doped $BaSnO_3$ in the literature [7,23,28,29,32,33]. As we dope with higher percentages of R^{3+} species, the overall lattice will expand as a result of charged point defects on the cation sublattice. This is counteracted by having substitutional dopants that are smaller than their host site, and so we only see a small increase in the lattice parameter in our doped $BaSnO_3$ films. From La-doping to Gd-doping, there is a slight change in the lattice constant of only about 0.2%. Since both dopants are trivalent, this further indicates that the lattice constant is more a function of defect concentration than substitutional cation size in these films.

TABLE I. Out-of-plane lattice constants for 8% rare-earth doped films as determined by x-ray diffraction. The FWHM of the rocking curves around the 002 Bragg reflection ($\Delta\omega$) are also given. The effective ionic radii of the dopants in a 12-fold coordination ($R^{3+}_{i,12}$) are used to calculate the *A*-site site mismatch as compared to Ba^{2+} ($r = 1.61$ Å by Shannon) [28,29]. The calculated ionic radii for the rare-earth cations are from Jia [30].

Dopant	a_{OOP} (Å)	$\Delta\omega_{002}$ (deg)	$R^{3+}_{i,12}$ (Å)	Site mismatch
La^{3+}	4.128 ± 0.004	0.060 ± 0.071	1.36	15.5%
Pr^{3+}	4.127 ± 0.003	0.039 ± 0.010	1.32	18.0%
Nd^{3+}	4.124 ± 0.004	0.073 ± 0.089	1.31	18.6%
Gd^{3+}	4.120 ± 0.004	0.041 ± 0.029	1.27	21.1%

PLD growth at different conditions can lead to films with comparable crystallinities (as determined by the rocking curve widths), but with vastly different functional properties. In early studies, La dopants had been incorporated into $BaSnO_3$ crystals of high quality, but high mobilities had not been achieved [31,34–42]. The newest wave of studies also shows a large variation in properties with the same nominal stoichiometries across different groups, and sometimes even within the same group [7–9,33,43–52]. We have found that microstructure alone is not always a good indicator of carrier mobilities in PLD-grown films [10,11,47,53].

Three parameters that had a significant impact on the resulting film properties were PLD target-to-substrate distance, oxygen growth pressure, and substrate choice. The target-to-substrate distance in PLD appears to strongly affect electrical transport in the resulting films. While generally it is preferable to keep the substrates further away from the high-energy plume in order to avoid resputtering of the film surface, we found that at distances of 3 in., the conduction turned off entirely. All of the films for which transport is shown in this study were grown at distances of 2.5 in. Next, we found that the ambient growth environment strongly influenced the conductivity, with high mobilities achieved at 100 mTorr O_2. Below 2 mTorr of oxygen, the films were quite insulating. Growing in oxygen pressures of 10^{-5} Torr led to high-quality films with low rocking curve widths, but even heavily doped $BaSnO_3$ films were insulating. Holding pressure constant at 100 mTorr but flowing a mixture of 99% N_2/1% O_2 instead of pure O_2 also yielded completely insulating films. This is somewhat surprising because oxygen vacancies should in theory be *n*-type dopants, and it has been shown that if undoped $BaSnO_3$ films are postannealed in vacuum, they can be made conducting [50,54]. The fact that growth in low oxygen pressures turns the conductivity off in PLD suggests that there are other compensating defects or unintended consequences to changing the growth pressure. Finally, we compared depositions on (001) $SrTiO_3$ substrates to those on (001) MgO substrates. While the difference between the rocking curve breadths of the films was very large—0.03–0.7 °C, respectively—there was virtually no difference in the electron mobilities.

This lack of correlation between microstructure and electronic properties suggests that either the dopants were not incorporated into the samples, or there were significant compensating defects such as cation vacancies or antisite defects.

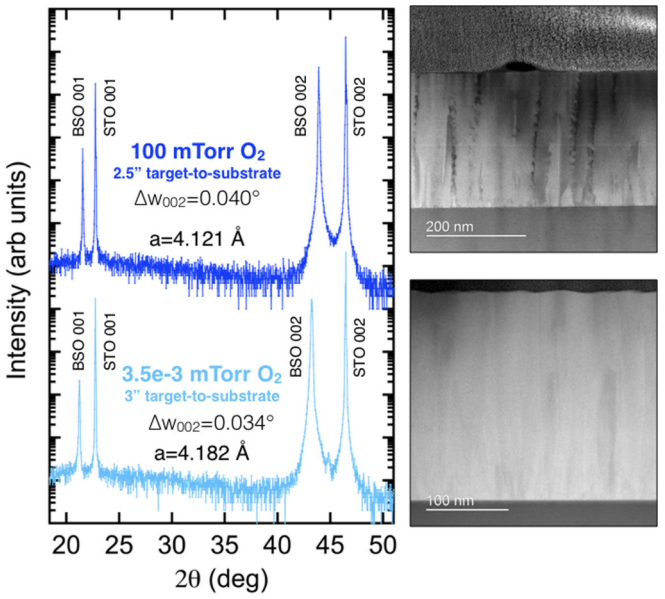

FIG. 2. Comparison between the structural quality of two 8% Gd-doped $BaSnO_3$ films that exhibit vastly different electronic transport. The top sample is conducting with $\mu = 12.2$ cm^2/V s and $\rho = 5.4$ mΩ, while the bottom sample is too insulating to measure in our transport system. The XRD spectra have been normalized by substrate intensity and shifted for clarity.

To investigate this further, we compared two Gd-doped films that had approximately the same full widths at half-maximum of their rocking curves but which had very different electronic transport properties. In this section, we will refer to them as the "conducting" film and the "insulating" film. The "conducting" film used the recipe outlined previously—a 2.5 in. target-to-substrate distance and an ambient pressure of 100 mTorr O_2. The "insulating film" was grown at a 3 in. target-to-substrate distance and an O_2 pressure of 3.5×10^{-3} mTorr. The temperature was held constant at 750 °C, and (001) $SrTiO_3$ substrates were used in both cases. The out-of-plane x-ray diffraction spectra are given in Fig. 2. Both show comparable crystallinity, with $\Delta\omega_{002} = 0.040°$ for the conducting film and $\Delta\omega_{002} = 0.034°$ for the insulating film. There is an expansion of the lattice parameter for the insulating case, perhaps as a result of additional charged defects such as oxygen vacancies.

The right-hand side of Fig. 2 shows the cross-sectional transmission electron microscopy (TEM) images for both films. Both show columnar grains; however, in the conducting sample there are large voids between the grains with a grain size of approximately 30–50 nm. These voids appeared to be deficient in both Ba and O. The surface quality was also quite different in both samples. The conducting films have patches of surface contrast at low magnifications that EDS identifies as barium oxide islands, whereas the insulating film appeared homogeneous even at higher magnifications. In both films, there were frequently lamellar defects that appeared as bright lines of contrast in dark-field imaging. Upon further inspection, they seemed to be regions of varying thickness in parts of the sample where islands that had nucleated separately began to impinge on one another.

We conducted energy-dispersive spectroscopy (EDS) in conjunction with cross-sectional TEM as shown in Fig. 3. Despite their very different electrical properties, both films had rare-earth dopants that were evenly interspersed throughout the samples. Thus, the lack of free carriers in the insulating film was not the result of dopant clustering or a lack of incorporation. In some cases, there were BaO islands on the surface of the conducting films, and Sn coated the voids between the grains as shown in the supplemental material [27]. No such features were observed in the insulating films.

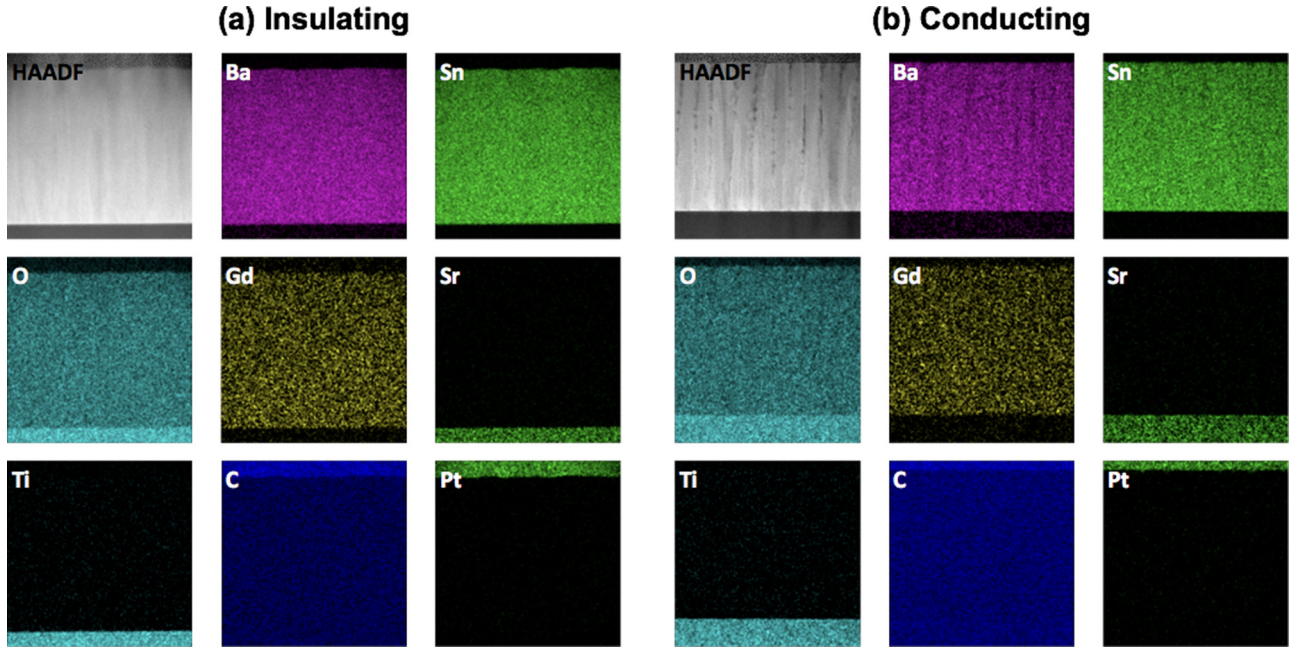

FIG. 3. Energy-dispersive spectroscopy of both the (a) "insulating" and (b) "conducting" 8% Gd-doped $BaSnO_3$ films measured in cross-sectional TEM shows homogeneous incorporation of the dopant atoms.

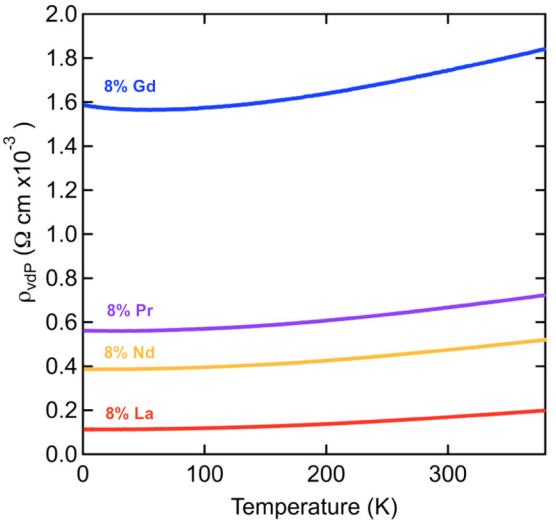

FIG. 4. Resistivity vs temperature for a few representative 8% Pr-, Nd-, and Gd-doped $BaSnO_3$ films in Fig. 5.

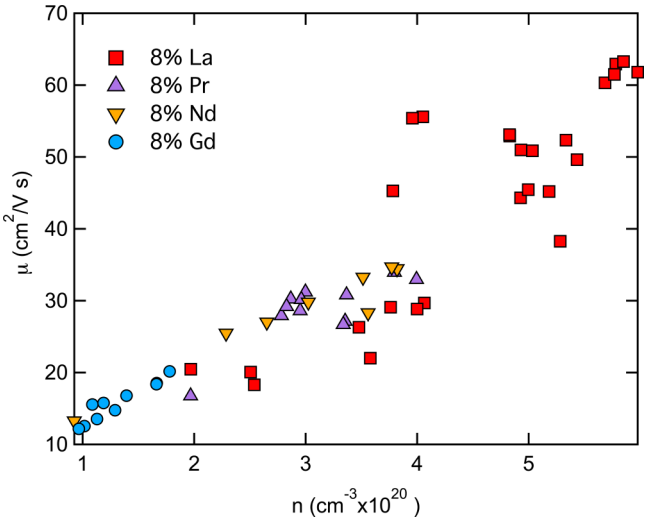

FIG. 5. Mobility vs carrier concentration for 8% Pr-, Nd-, and Gd-doped $BaSnO_3$ films at room temperature. All films in this plot have thicknesses of approximately 300 nm.

It is surprising that the film with (slightly) higher $\Delta\omega$ values and with extensive microstructural defects as seen in TEM can have the excellent transport properties that will be discussed in Sec. III B.

B. Electronic transport

All of the dopants tested in $BaSnO_3$ were *n*-type, yielding high room-temperature mobilities and conductivities when grown in 100 mTorr O_2 and with a 2.5 in. target-to-substrate distance. Only films grown in oxygen-poor ambient conditions or at larger target-to-substrate distances are insulating. The doped BSO films are metallic (i.e., $\frac{d\rho}{dt} > 0$) across the temperature range 2–380 K; however, the resistivity versus temperature curves are still quite flat, as shown in Fig. 4. This indicates that phonon scattering does not play an important role in the transport of these films and that scattering from ionized impurities is the dominant mechanism limiting the resistivity. This is consistent with other reports in the literature, where degenerately doped $BaSnO_3$ is not significantly affected by changes in temperature [10–12,25]. All films do exhibit a flattening of the resistivity curve and a slight upturn at lower temperatures. This has also been observed across multiple studies on the $BaSnO_3$ system and is sometimes attributed to weak localization. In our case, the increase in resistivity is coincident with a decrease in carrier concentration. All films exhibit a small negative magnetoresistance, measured with the applied field perpendicular to the sample plane, at low temperatures. This behavior can arise from the presence of strong paramagnetic moments.

Of the dopants in this study, La-doping of $BaSnO_3$ resulted in the highest mobilities, with values as high as 65 cm^2/V s. As the ionic radii of the dopant species decrease from La down to Gd (see Table I), the typical mobility values correspondingly decrease despite the films having similar crystalline quality. One likely explanation is that the larger the site mismatch with the native Ba site, the more pronounced the local strain fields that would serve to limit the carrier mobilities. Different activation energies may also account for this behavior. Typical room-temperature mobilities for La-, Pr-, Nd-, and Gd-doped $BaSnO_3$ films are shown in Fig. 5 and tabulated in Table II.

All of the rare-earth doped samples appear to lie along the same carrier concentration (n) versus mobility (μ) curve as the La-doped samples, although with lower mobilities and carrier concentrations overall. They are well-segregated by n, so fewer carriers seem to be activated with higher-Z (lower ionic radius) dopants. The Gd-doped samples are clustered in the bottom-left corner of the plot, with the lowest mobilities and carrier concentrations. As we noted previously, Gd^{3+} has the greatest size mismatch with the host Ba^{2+} site. This could lead to local strain fields around the *A*-sites and cause a decrease in mobility. Another possibility is that with smaller cations, there is a greater probability of *B*-site occupation. Scanlon has calculated that after oxygen vacancies, antisite defects have the lowest formation energies in $BaSnO_3$ [55]. Therefore, antisite disorder is a possible explanation. Similar arguments can be made for Pr- and Nd-doped samples as compared to La-doped samples.

Other reports on doped $BaSnO_3$ thin films also show a positive trend between carrier concentration and mobility [10–12,56]. This correlation indicates that grain boundaries and dislocations that are introduced concurrently with aliovalent dopants serve to both scatter and trap carriers simultaneously. That is, there may be a screening effect that occurs within the material; once dislocations are sufficiently

TABLE II. Representative transport properties for each doping scheme.

Dopant 8%	$\rho^{vdP}_{300\,K}$ (mΩ cm)	$\mu_{300\,K}$ (cm^2/V s)	$n_{300\,K}$ (10^{20} cm^{-3})	ℓ (nm)
La	0.169	63.3	5.85	11
Pr	0.484	34.0	3.80	5.0
Nd	0.477	34.7	3.77	5.1
Gd	1.74	20.2	1.78	2.3

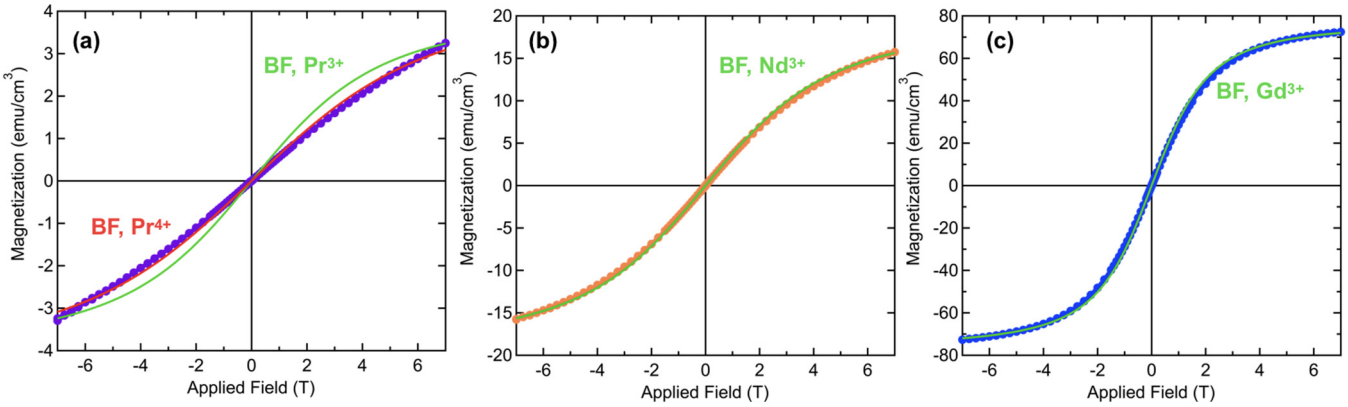

FIG. 6. SQUID magnetometry results at 4.5 K for (a) 8% Pr, (b) 8% Nd, and (c) 8% Gd-doped $BaSnO_3$. The green lines represent the Brillouin functions for the trivalent ions. In (a), both the trivalent (Pr^{3+}, green) and tetravalent (Pr^{4+}, red) cases are plotted.

compensated through trapping of electrons, additional carriers added to the system may scatter from impurities, but the defects have already been compensated so there is no loss of mobility with increased carrier concentration.

Given that we have found that our films have a small grain size on the order of 30–50 nm, we can compare this with the mean free path as calculated from $\ell = v_F\tau = \frac{\hbar\mu}{e}(3\pi^2 n)^{1/3}$. The calculated mean free paths are given in Table II. For the La-doped sample, ℓ is about a third of the grain size, while for Gd-doping, the mean free path is an order of magnitude smaller than the grain size measured by TEM. These mobilities are then reasonable values. Furthermore, it explains why larger grain sizes do not significantly impact electrical transport in these films. Together these results suggest that point defects and ionized impurities are more relevant to mobility-limiting mechanisms than grain-boundary scattering.

C. Magnetism

We probed the magnetic response of the films using SQUID magnetometry and x-ray magnetic circular dichroism. To minimize the possibility of having spurious signals on the order of the intrinsic magnetic moment (i.e., due to magnetic dust or other extrinsic impurities), the films measured by SQUID magnetometry were grown to thicknesses of $\sim$3 μm. Magnetic moment versus field curves are given in Fig. 6 for 8% Pr-, Nd-, and Gd-doping schemes. Samples were field-cooled from room temperature in 7 T and measured at 4.5 K. In each of the curves, there is a strong paramagnetic signal with a characteristic S-shaped curve.

We modeled the magnetization in these samples in terms of noninteracting spins as described by $M = M_s B_J(y)$, where $M_s = ng_J\mu_B J$, where $B_J(y)$ is the Brillouin function, n is the number of magnetic moments per unit volume, J is the angular momentum, and g_J is the Landé g-factor $g_J = \frac{3}{2} + \frac{S(S+1)-L(L+1)}{2J(J+1)}$. The Brillouin functions for the trivalent dopant ions are plotted in green in Fig. 4. We set the function to match the magnitude of the data at 7 T, and fit for the first derivative. The shape of the magnetic response is well-described by this relation for the Nd^{3+} and Gd^{3+} cases. However, the measured data fall short of the predicted Pr^{3+} response. The slope about the origin is better described by the Pr^{4+} function (given by the red line in Fig. 4, which is a $4f^1$ system). While most of the rare-earth ions are trivalent, both Pr^{4+} with an electron configuration of $4f^1 5d^0 6s^0$ and Pr^{3+} with $4f^2 5d^0 6s^0$ are stable depending on the surrounding environment. For example, $PrCoO_3$ is primarily in a Pr^{3+} valence state, but below its spin state transition there is a charge transfer between the cations resulting in a detectable amount of Pr^{4+} in the x-ray absorption spectroscopy spectra [57–60]. Pr can also be found on the B-site in an octahedral environment. $BaPrO_3$ is a stable compound that can exhibit long-range magnetic order arising from exchange between Pr^{4+} cations [61,62]. It has also been shown that when Pr is doped into $BaXO_3$-type compounds, it can be tetravalent and occupy the X-site. Hinatsu *et al.* showed that $BaCeO_3$, $BaZrO_3$, $BaHfO_3$, and even $BaSnO_3$ can each have Pr^{4+} substitutionally dope the tetravalent B-site. This isovalent doping scheme leads to an increase of the lattice parameter [63–65].

To investigate whether there is evidence for Pr^{4+} in our doped $BaSnO_3$ samples, we conducted x-ray absorption spectroscopy (XAS) and x-ray magnetic circular dichroism (XMCD) experiments at $\sim$20 K around the rare-earth $M_{5,4}$ edges, as shown in Fig. 7. The M-edges probe transitions from the $3d$ states to the unoccupied $4f$ levels. Comparing experimental reference spectra for Pr^{3+} and Pr^{4+}, we see that the peaks in Fig. 7(a) near the (ii) and (iii) markers are indicative of Pr^{3+} on the perovskite A-site in oxides. Pr^{4+} in an octahedral environment gives broad features at energies corresponding to (i) and (iv) in $BaPrO_3$ [57,60]. While we do not see any notable signatures at (i), there is a small feature at (iv) in our data that is consistent with some amount of Pr^{4+} in the Pr-doped samples. XAS is also a surface-sensitive technique, and therefore it would not be able to detect Pr^{4+} deeper within the film. The XAS features observed in the Nd- and Gd-doped samples are very similar to calculated spectra for the trivalent state [66–68].

A nonzero XMCD signal was observed in all samples on the $M_{4,5}$ edges of the lanthanide dopants. All measurements were taken at $\pm$0.5 T and are given in the ($\uparrow\downarrow - \uparrow\uparrow$) convention; the change in sign of the XMCD signal from Pr and Nd to Gd is a result of differences between half-filled and less than half-filled orbitals. For rare-earth elements with the $4f$ less than half-filled, $J = |L - S|$; however, for rare-earth elements with the $4f$ half-filled or more than half-filled (Gd and above), $J = |L + S|$. This is reflected in calculations

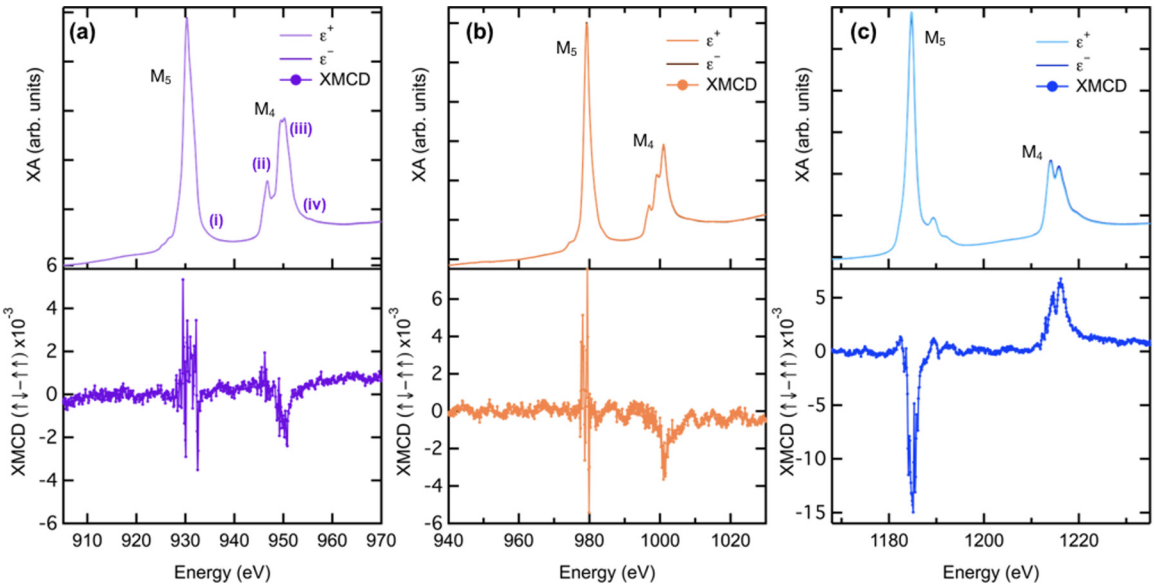

FIG. 7. X-ray absorption and x-ray magnetic circular dichroism measurements at ∼20 K on (a) Pr M_{45} edge for 8% Pr, (b) Nd M_{45} edge for 8% Nd, and (c) Gd M_{45} edge for 8% Gd-doped $BaSnO_3$ films. The lower-energy peak for all samples is the M_5 while the higher-energy XAS peak corresponds to the M_4 transition. Measurements were conducted on Beamline 4.0.2 of the Advanced Light Source with an applied magnetic field for XMCD measurements of ±0.5 T.

by Goedkoop and others [67,68]. The larger XMCD signal for the Gd-doped sample is a result of a greater difference between spin-up and spin-down transition probabilities in Gd. Since Gd^{3+} is a $4f^7$ system, each of the seven electrons is unpaired and will minimize their energy if they have the same spin. Due to the weaker signal of Pr^{3+} and Nd^{3+}, some fluctuations in the background intensity of the XMCD spectra are observable. (These are artifacts and do not correspond to actual transitions.) Magnetic-field loops between ±0.5 T were taken on the M_5 edge, and exhibit no observable hysteresis in the XMCD.

Together these results suggest that our Pr-, Nd-, and Gd-doped $BaSnO_3$ samples are paramagnetic with no long-range magnetic ordering. In the case of Pr-doping, there is evidence to suggest that the films may have some quantity of Pr^{4+}, which would serve to reduce the observed magnetic signal. In the case of our Nd-doped samples, we believe the $BaSnO_3$ is doped with Nd^{3+} on the Ba site. While there are some reports in the literature that Nd can be divalent, our spectra contain all of the features of Nd^{3+} and our SQUID results are well-fit by assuming a contribution to the signal only from trivalent cations. In our Gd-doped samples, the spectral shape of the Gd M-edge is very similar to other Gd^{3+}-containing compounds. Furthermore, the Brillouin function for Gd^{3+} describes the SQUID magnetometry field dependence quite well.

D. Optical properties

The optical properties of the films were measured using ellipsometry. The dielectric constant ε_2 for a $SrTiO_3$ substrate and an 8% La-doped $BaSnO_3$ film on a $SrTiO_3$ substrate are plotted in Figs. 8(a) and 8(b). Models for interpretation of ε_2 were built using Woollam's WVASE32 software. Each model consisted of Drude and Tauc-Lorenz "oscillators," or functional forms, in series to describe the predicted response from the Fresnel equations which depend on the optical constants and the thickness of the materials. These oscillators are plotted as dashed lines in Figs. 8(a) and 8(b). For the $SrTiO_3$ substrate, there are some deviations from ideal $SrTiO_3$, which are compensated by adding a third Tauc-Lorentz oscillator with a broad functional form.

The shape of ε_2 is quite different for 8% La-doped $BaSnO_3$ compared to the substrate. The conducting films show a significant Drude tail at low energies as a result of introducing free carriers into the material, an observation that is consistent with our electrical transport results. The first band-to-band transition in the 8% La-doped film occurs at a higher energy than in $SrTiO_3$ and is also weaker in intensity. This likely stems from the lower density of states for the 5s-derived conduction band, as compared to the 3d conduction band in $SrTiO_3$. The Sn 5s has a lower band degeneracy than the Ti 3d; since we are essentially probing the probability of transition from the O 2p to the conduction band, the intensity of ε_2 will be higher for transition-metal oxides than for compounds that have conduction bands with strong s character.

We also notice that the onset of absorption in $BaSnO_3$ occurs at higher energies than for $SrTiO_3$, indicating that $BaSnO_3$ has a larger band gap than the substrate. This is consistent with the literature, where $SrTiO_3$ is reported to have a band gap of approximately 3.2 eV and $BaSnO_3$ is reported to have a band gap in the range of 3–4 eV [6,43,69–71]. Since the substrate is more strongly absorbing than the film in this system and also has more features, it is useful to derive the transmittance from reflection measurements (as with ellipsometry) rather than from transmission measurements (as with uv-vis spectroscopy). For this reason, we have calculated the transmittance for the doped BSO films only by subtracting the contribution from the underlying $SrTiO_3$ substrate.

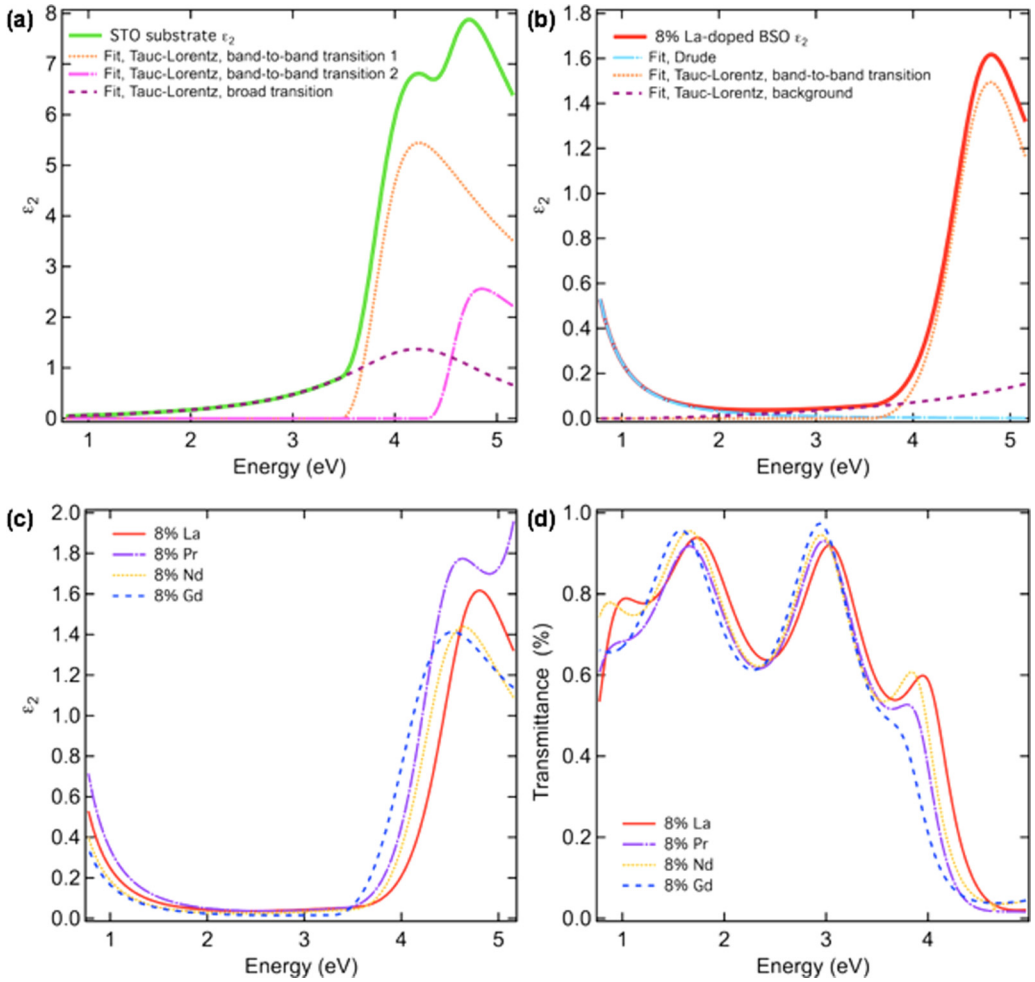

FIG. 8. Optical properties of the $SrTiO_3$ substrate and doped $BaSnO_3$ films. (a) ε_2 of the $SrTiO_3$ substrate with the oscillators used to construct the model. (b) ε_2 of an 8% La-doped $BaSnO_3$ film with individual model components shown. (c) ε_2 for the same 8%-doped La film compared with films doped with 8% Pr, 8% Nd, and 8% Gd. (d) Transmittance for freestanding $BaSnO_3$ 200 nm films as calculated from optical constants.

Transmittance curves for 200 nm doped freestanding $BaSnO_3$ films alone are calculated from the extracted BSO optical constants and shown in Fig. 8(d). The oscillations are a function of film thickness. There are no notable differences between the transmittance of films with different rare-earth dopants. All are fairly transparent across the visible range despite being quite thick and degenerately doped.

IV. DISCUSSION

In our films, we find that microstructural quality is not a good predictor of conductivity. Instead, growth conditions such as oxygen pressure and target-to-substrate distance play a dominant role in determining the electrical transport of the films. Since microstructure is not the limiting factor in the conductivity, point defects likely cause the vast changes in mobility, carrier concentration, and resistivity values. Not only have we found that microstructure does not track neatly with transport, but we also show through TEM with EDS that dopants can be well-dispersed throughout samples without leading to any measurable conduction. Electrical conduction can be completely turned off simply by decreasing the oxygen pressure or changing the target-to-substrate distance. Together with the literature on $BaSnO_3$ prior to 2012, our study offers further evidence that point defects are affecting the transport in ways that are difficult to detect [31,34–42].

When a trivalent rare-earth (R) element substitutes for Ba^{2+}, there *must* be some way to maintain crystal neutrality. In the ideal case, $R^{\bullet}_{Ba}$ is compensated by delocalized electrons (e'), but there are other negatively charged defects that could form instead. Negatively charged defects that in theory could form in doped $BaSnO_3$ films are oxygen interstitials (O''_i), cation vacancies (V''_{Ba}, V''''_{Sn}), and antisite defects (Ba''_{Sn}). Site mixing of rare-earth dopants could also play a role in parasitic compensation (e.g., Gd'_{Sn}). For completeness, we list possible positively charged defects that could potentially enhance n-type conduction or screen negatively charged point defects: $V^{\bullet\bullet}_{O}$, $Ba^{\bullet\bullet}_{i}$, $Sn^{\bullet\bullet\bullet\bullet}_{i}$, $Sn^{\bullet\bullet}_{Ba}$, $R^{\bullet\bullet\bullet}_{i}$, $R^{\bullet}_{Ba}$. We note that we also conducted XAS on the oxygen K-edge for these doped $BaSnO_3$ films, but we did not detect any major change in the line shape between conducting and insulating films, or between La-, Pr-, Nd-, and Gd-doping schemes (see the Supplementary Material [27]).

We consider each of the proposed negatively charged defects individually. While it has been calculated that oxygen interstitials actually have low formation energies in $BaSnO_3$, it is predicted that they will relax toward lattice oxygen sites and form local peroxide groups [55]. Higher oxygen pressures during growth actually aid conduction in our case, and O_i'' are acceptor-like defects. For this reason, cationic vacancies are a more likely scenario. Prakash *et al.* deliberately engineered barium vacancies in their highly conducting films grown by hybrid-MBE [53]. In our TEM and EDS results, we see that there are BaO islands on the surface of the conducting films but not the insulating ones (see the Supplemental Material [27]). So, it seems likely that V_{Ba}'' could occur. However, Scanlon reports that in theory, oxygen-rich conditions serve to compensate *n*-type conduction [55]. We observe the opposite case; higher oxygen pressures are *more* likely to stabilize *n*-type conducting films. Still, the basic premise that V_{Ba}'' is a low-energy defect may be relevant. In terms of V_{Sn}'''', Coey *et al.* and others have reported that Sn is a volatile species in pulsed laser deposition, and that the target-to-substrate distance can influence the incorporation of Sn [21,72]. Since closer target-to-substrate distances lead to higher conductivities and potentially more Sn, V_{Ba}'' may play a role in the insulating nature of films grown with large target-to-substrate distances. Finally, we consider the antisite defect Ba_{Sn}''. Solely predicated on size considerations, there is a large mismatch between these dopants. Twelvefold-coordinated Ba^{2+} has an ionic radius of 1.61 Å while octahedrally coordinated Sn^{4+} has an ionic radius of 0.69 Å. In a strictly stoichiometric compound, the occurrence of Ba_{Sn}'' may be unlikely. However, it has been reported that due to the large size of the *A*-site in $BaSnO_3$, the Sn cations may actually reside on the *A*-sites and take a divalent oxidation state to form Sn_{Ba}^{x} [36,40,55,73]. While the defect itself is charge-neutral, site balance requirements can induce charged cationic vacancies, thereby suppressing conductivity in our doped films.

Another puzzling feature of our findings is that growth in low oxygen pressures by PLD suppresses conductivity, even though it has been theoretically predicted that oxygen vacancies are an *n*-type dopant, and it has been experimentally shown that postgrowth annealing in vacuum can lead to conduction and high electron mobilities [50,54,55]. Clearly, growth by PLD in low oxygen pressures has unintended consequences. The need for high growth pressures as well as a close target-to-substrate distance suggests that in PLD growth of $BaSnO_3$, the region of the plume that is sampled by the substrate is critical to generating the point defects that lead to conduction instead of compensating species.

Finally, we consider the differences in conduction between different dopants in our study. La-doping clearly leads to the most desirable transport properties for traditional uses of transparent conducting oxides. The PLD-grown La-doped samples have the highest mobilities of the samples in this study, reaching as high as $\mu = 65\ \mathrm{cm^2/V\,s}$ at room temperature. They are thus comparable to existing literature on La-doped $BaSnO_3$ films grown by pulsed laser deposition [4,8,56], although films grown by molecular beam epitaxy have shown higher electron mobilities [10–12]. Gd-doping leads to the lowest conductivities and mobilities. It may be that the size mismatch between Gd^{3+} and Ba^{2+} causes the rare earth to preferentially sit on the Sn^{4+} sites. Then, Gd_{Sn}' could compensate $Gd_{Ba}^{\bullet}$. In the La-doped system, theoretical predictions do suggest that under some circumstances [74], La_{Sn}' is low-energy and can compensate $La_{Ba}^{\bullet}$, so this is certainly a possibility [55]. Despite the larger size of Pr^{3+} compared to Nd^{3+}, Pr-doped films have comparable, and perhaps lower, mobilities than Nd-doped films. Pr^{4+} can exist and substitute for Sn^{4+} as we have discussed, so that is one potential mechanism for the lower conduction and additional band in the ellipsometry data for Pr-doped films. There is also some evidence for the existence of Pr^{4+} in SQUID magnetometry and XMCD.

With respect to magnetic doping, it appears that Gd- and Nd-doping are more promising than Pr for this reason. Both Gd and Nd are stable in the trivalent state, which is more desirable so as to maximize *S*. Though the dopants led to paramagnetism and there is no evidence for long-range order, there is some room for improvement. Because the slope of the *n* versus μ curve is positive, we reason that it is possible to both increase the conductivity by adding more dopants while also increasing magnetic response.

V. CONCLUSION

In summary, we have demonstrated transparency, high mobility, and paramagnetism in 8% Pr-, Nd-, and Gd-doped epitaxial $BaSnO_3$ thin films. The larger the dopant size mismatch with the Ba site, the smaller the carrier concentrations and electron mobilities. The crystallinity of the thin-film samples does not appear to be the main limiter of the electron mobilities, and we have also shown that in PLD-grown $BaSnO_3$ films, the mean free path is smaller than the grain size. Both bulk magnetometry and XMCD measurements show that these epitaxial films exhibit strong paramagnetic signals with no evidence of long-range order. The positive trend of magnetic dopant concentrations with carrier mobilities in all rare-earth doped films in this study shows that opportunities remain to increase *both* the mobility and the magnetization in these films with higher doping concentrations in the quest toward a new class of ferromagnetic semiconductors.

ACKNOWLEDGMENTS

We thank Purnima P. Balakrishnan, Charles L. Flint, Matthew T. Gray, Michael J. Veit, and Useong Kim for useful discussions. This work was supported by the National Science Foundation under Award No. 1762971. Part of this work was performed at the Stanford Nano Shared Facilities (SNSF), supported by the National Science Foundation under Award No. ECCS-1542152. Additional support was granted by the Chemical Imaging Initiative, a Laboratory Directed Research and Development Program at Pacific Northwest National Laboratory (PNNL). PNNL is a multiprogram national laboratory operated by Battelle for the U.S. Department of Energy (DOE) under Contract No. DE-AC05-76RL01830. A portion of the research was performed using the Environmental Molecular Sciences Laboratory (EMSL), a national scientific user facility sponsored by the Department of Energy's Office of Biological and Environmental Research and located at PNNL.

RBS was carried out in the Characterization Facility, University of Minnesota, which receives partial support from NSF through the MRSEC program. The work at UMN acknowledges support from the Air Force Office of Scientific Research (AFOSR) through Grant No. FA9550-19-1-0245. This research used resources of the Advanced Light Source, which is a DOE Office of Science User Facility under Contract No. DE-AC02-05CH11231.

[1] T. Ohnishi, K. Shibuya, T. Yamamoto, and M. Lippmaa, Defects and transport in complex oxide thin films, J. Appl. Phys. **103**, 103703 (2008).

[2] J. Son, P. Moetakef, B. Jalan, O. Bierwagen, N. J. Wright, R. Engel-Herbert, and S. Stemmer, Epitaxial $SrTiO_3$ films with electron mobilities exceeding 30 000 $cm^2\ V^{-1}\ s^{-1}$, Nat. Mater. **9**, 482 (2010).

[3] *Multifunctional Oxide Heterostructures*, edited by E. T. Tsymbal, E. Dagotto, C. B. Eom, and R. Ramesh (Oxford University Press, Oxford, 2012).

[4] S. Ismail-Beigi, F. J. Walker, S.-W. Cheong, K. M. Rabe, and C. H. Ahn, Alkaline earth stannates: The next silicon? APL Mater. **3**, 062510 (2015).

[5] T. A. Cain, A. P. Kajdos, and S. Stemmer, La-doped $SrTiO_3$ films with large cryogenic thermoelectric power factors, Appl. Phys. Lett. **102**, 182101 (2013).

[6] X. Luo, Y. S. Oh, A. Sirenko, P. Gao, T. A. Tyson, K. Char, and S.-W. Cheong, High carrier mobility in transparent $Ba_{1-x}La_xSnO_3$ crystals with a wide band gap, Appl. Phys. Lett. **100**, 172112 (2012).

[7] H. J. Kim, U. Kim, H. M. Kim, T. H. Kim, H. S. Mun, B.-G. Jeon, K. T. Hong, W.-J. Lee, C. Ju, K. H. Kim, and K. Char, High mobility in a stable transparent perovskite oxide, Appl. Phys. Exp. **5**, 061102 (2012).

[8] H. J. Kim, U. Kim, T. H. Kim, J. Kim, H. M. Kim, B. G. Jeon, W. J. Lee, H. S. Mun, K. T. Hong, J. Yu, K. Char, and K. H. Kim, Physical properties of transparent perovskite oxides (Ba, La)SnO_3 with high electrical mobility at room temperature, Phys. Rev. B **86**, 165205 (2012).

[9] W.-J. Lee, H. J. Kim, J. Kang, D. H. Jang, T. H. Kim, J. H. Lee, and K. H. Kim, Transparent perovskite barium stannate with high electron mobility and thermal stability, Annu. Rev. Mater. Res. **47**, 391 (2017).

[10] S. Raghavan, T. Schumann, H. Kim, J. Y. Zhang, T. A. Cain, and S. Stemmer, High-mobility $BaSnO_3$ grown by oxide molecular beam epitaxy, APL Mater. **4**, 016106 (2016).

[11] H. Paik, Z. Chen, E. Lochocki, H. Ariel Seidner, A. Verma, N. Tanen, J. Park, M. Uchida, S. Shang, B. Cheng Zhou, M. Brützam, R. Uecker, Z. K. Liu, D. Jena, K. M. Shen, D. A. Muller, and D. G. Schlom, Adsorption-controlled growth of La-doped $BaSnO_3$ by molecular-beam epitaxy, APL Mater. **5**, 116107 (2017).

[12] A. Prakash, P. Xu, A. Faghaninia, S. Shukla, J. W. Ager III, C. S. Lo, and B. Jalan, Wide bandgap $BaSnO_3$ films with room temperature conductivity exceeding 104 S cm^{-1}, Nat. Commun. **8**, 15167 (2017).

[13] Z. Lebens-Higgins, D. O. Scanlon, H. Paik, S. Sallis, Y. Nie, M. Uchida, N. F. Quackenbush, M. J. Wahila, G. E. Sterbinsky, Dario A. Arena, J. C. Woicik, D. G. Schlom, and L. F. J. Piper, Direct Observation of Electrostatically Driven Band Gap Renormalization in a Degenerate Perovskite Transparent Conducting Oxide, Phys. Rev. Lett. **116**, 027602 (2016).

[14] O. Parkash, D. Kumar, K. K. Srivastav, and R. K. Dwivedi, Electrical conduction behavior of cobalt substituted $BaSnO_3$, J. Mater. Sci. **36**, 5805 (2001).

[15] K. Balamurugan, N. H. Kumar, J. A. Chelvane, and P. N. Santhosh, Room temperature ferromagnetism in Fe-doped $BaSnO_3$, J. Alloys Comp. **472**, 9 (2009).

[16] K. Balamurugan, N. Harish Kumar, B. Ramachandran, M. S. Ramachandra Rao, J. Arout Chelvane, and P. N. Santhosh, Magnetic and optical properties of Mn-doped $BaSnO_3$, Solid State Commun. **149**, 884 (2009).

[17] Q. Liu, Y. He, H. Li, B. Li, G. Gao, L. Fan, and J. Dai, Room-temperature ferromagnetism in transparent Mn-doped $BaSnO_3$ epitaxial films, Appl. Phys. Exp. **7**, 033006 (2014).

[18] K. K. James, A. Aravind, and M. K. Jayaraj, Structural, optical and magnetic properties of Fe-doped barium stannate thin films grown by PLD, Appl. Surf. Sci. **282**, 121 (2013).

[19] U. S. Alaan, A. T. N'Diaye, P. Shafer, E. Arenholz, and Y. Suzuki, Structure and magnetism of Fe-doped $BaSnO_3$ thin films, AIP Adv. **7**, 055716 (2017).

[20] D.-S. Gao, X.-D. Gao, Y.-Q. Wu, T.-T. Zhang, J.-N. Yang, and X.-M. Li, Epitaxial Co-doped $BaSnO_3$ thin films with tunable optical bandgap on MgO substrate, Appl. Phys. A **125**, 158 (2019).

[21] J. M. D. Coey, A. P. Douvalis, C. B. Fitzgerald, and M. Venkatesan, Ferromagnetism in Fe-doped SnO_2 thin films, Appl. Phys. Lett. **84**, 1332 (2004).

[22] K. Balamurugan, N. Harish Kumar, J. Arout Chelvane, and P. N. Santhosh, Effect of W co-doping on the optical, magnetic and electrical properties of Fe-doped $BaSnO_3$, Physica B **407**, 2519 (2012).

[23] U. S. Alaan, P. Shafer, A. T. N'Diaye, E. Arenholz, and Y. Suzuki, Gd-doped $BaSnO_3$: A transparent conducting oxide with localized magnetic moments, Appl. Phys. Lett. **108**, 042106 (2016).

[24] E. McCalla, D. Phelan, M. J. Krogstad, B. Dabrowski, and C. Leighton, Electrical transport, magnetic and thermodynamic properties of La, Pr and Nd doped $BaSnO_{3-\delta}$ single crystals, Phys. Rev. Mater. **2**, 084601 (2018).

[25] F.-Y. Fan, W.-Y. Zhao, T.-W. Chen, J.-M. Yan, J.-P. Ma, L. Guo, G.-Y. Gao, F.-F. Wang, and R.-K. Zheng, Excellent structural, optical, and electrical properties of Nd-doped $BaSnO_3$ transparent thin films, Appl. Phys. Lett. **113**, 202102 (2018).

[26] While the films are generally of good quality, there were some cases in which other phases occurred. Most notably, a small peak may appear in between the film and substrate 002 reflections near ∼45°. We attribute this to the 002 or 202 Ba_2SnO_4 phase. For some depositions, a BSO 111 reflection was also observed. There did not appear to be a correlation with the observation of these secondary phases; they appeared occasionally in all doping schemes.

[27] See Supplemental Material at http://link.aps.org/supplemental/10.1103/PhysRevMaterials.3.124402 for more details on

out-of-plane constants for all samples, additional TEM and EDS data, and more details on oxygen K-edge XAS.

[28] R. D. Shannon and C. T. Prewitt, Effective ionic radii in oxides and fluorides, Acta Crystallogr. Sect. B **25**, 925 (1969).

[29] R. D. Shannon, Revised effective ionic radii and systematic studies of interatomic distances in halides and chalcogenides, Acta Crystallogr. Sect. A **32**, 751 (1976).

[30] Y. Q. Jia, Crystal radii and effective ionic radii of the rare earth ions, J. Solid State Chem. **95**, 184 (1991).

[31] T. Huang and M. Itoh, Electrical properties of $BaSnO_3$ in substitution of antimony for tin and lanthanum for barium, J. Mater. Sci. **30**, 1556 (1995).

[32] M. Leszczyński, E. Litwin-Staszewska, T. Suski, J. Bak-Misiuk, and J. Domagala, Lattice constant of doped semiconductor, Acta Phys. Pol. A **88**, 837 (1995).

[33] P. V. Wadekar, J. Alaria, M. O'Sullivan, N. L. O. Flack, T. D. Manning, L. J. Phillips, K. Durose, O. Lozano, S. Lucas, J. B. Claridge, and M. J. Rosseinsky, Improved electrical mobility in highly epitaxial La:$BaSnO_3$ films on $SmScO_3$(110) substrates, Appl. Phys. Lett. **105**, 052104 (2014).

[34] M. G. Smith, J. B. Goodenough, A. Manthiram, R. D. Taylor, W. Peng, and C. W. Kimball, Tin and antimony valence states in $BaSn_{0.85}Sb_{0.15}O_{3-\delta}$, J. Solid State Chem. **98**, 181 (1992).

[35] M. Trari, J.-P. Doumerc, P. Dordor, M. Pouchard, G. Behr, and G. Krabbes, Preparation and characterization of lanthanum doped $BaSnO_3$, J. Phys. Chem. Solids **55**, 1239 (1994).

[36] B. Hadjarab, A. Bouguelia, and M. Trari, Optical and transport properties of lanthanum-doped stannate $BaSnO_3$, J. Phys. D **40**, 5833 (2007).

[37] M. Yasukawa, T. Ikeuchi, K. Kono, H. Yanagi, and H. Hosono, Preparation of semiconductive La-doped $BaSnO_3$ by a polymerized complex method and the thermoelectric properties, J. Jpn. Soc. Powder Metall. **54**, 639 (2007).

[38] H. F. Wang, Q. Z. Liu, F. Chen, G. Y. Gao, W. Wu, and X. H. Chen, Transparent and conductive oxide films with the perovskite structure: La- and Sb-doped $BaSnO_3$, J. Appl. Phys. **101**, 106105 (2007).

[39] D. Y. Wang, J. Wang, H. L. W. Chan, and C. L. Choy, Structural and electro-optic properties of $Ba_{0.7}Sr_{0.3}TiO_3$ thin films grown on various substrates using pulsed laser deposition, J. Appl. Phys. **101**, 043515 (2007).

[40] B. Hadjarab, A. Bouguelia, A. Benchettara, and M. Trari, The transport and photo electrochemical properties of La-doped $BaSnO_3$, J. Alloys Comp. **461**, 360 (2008).

[41] M. Yasukawa, T. Kono, K. Ueda, H. Yanagi, and H. Hosono, High-temperature thermoelectric properties of La-doped $BaSnO_3$ ceramics, Mater. Sci. Eng. B **173**, 29 (2010).

[42] Q. Liu, J. Liu, B. Li, H. Li, G. Zhu, K. Dai, Z. Liu, P. Zhang, and J. Dai, Composition dependent metal-semiconductor transition in transparent and conductive La-doped $BaSnO_3$ epitaxial films, Appl. Phys. Lett. **101**, 241901 (2012).

[43] K. K. James, P. S. Krishnaprasad, K. Hasna, and M. K. Jayaraj, Structural and optical properties of La-doped $BaSnO_3$ thin films grown by PLD, J. Phys. Chem. Solids **76**, 64 (2015).

[44] U. Kim, C. Park, T. Ha, Y. M. Kim, N. Kim, C. Ju, J. Park, J. Yu, J. H. Kim, and K. Char, All-perovskite transparent high mobility field effect using epitaxial $BaSnO_3$ and $LaInO_3$, APL Mater. **3**, 036101 (2015).

[45] R. H. Wei, X. W. Tang, Z. Z. Hui, X. Luo, J. M. Dai, J. Yang, W. H. Song, L. Chen, X. G. Zhu, X. B. Zhu, and Y. P. Sun, Solution processing of transparent conducting epitaxial La:$BaSnO_3$ films with improved electrical mobility, Appl. Phys. Lett. **106**, 101906 (2015).

[46] W.-J. Lee, H. J. Kim, E. Sohn, T. H. Kim, J.-Y. Park, W. Park, H. Jeong, T. Lee, J. H. Kim, K.-Y. Choi, and K. H. Kim, Enhanced electron mobility in epitaxial (Ba, La)SnO_3 films on $BaSnO_3$(001) substrates, Appl. Phys. Lett. **108**, 082105 (2016).

[47] J. Shiogai, K. Nishihara, and A. Sato, and K. Tsukazaki, Improvement of electron mobility in La:$BaSnO_3$ thin films by insertion of an atomically flat insulating (Sr, Ba)SnO_3 buffer layer, AIP Adv. **6**, 065305 (2016).

[48] S. Yu, D. Yoon, and J. Son, Enhancing electron mobility in La-doped $BaSnO_3$ thin films by thermal strain to annihilate extended defects, Appl. Phys. Lett. **108**, 262101 (2016).

[49] C. A. Niedermeier, S. Rhode, S. Fearn, K. Ide, M. A. Moram, H. Hiramatsu, H. Hosono, and T. Kamiya, Solid phase epitaxial growth of high mobility La:$BaSnO_3$ thin films co-doped with interstitial hydrogen, Appl. Phys. Lett. **108**, 172101 (2016).

[50] K. Ganguly, B. Prakash, A. Jalan, and C. Leighton, Mobility-electron density relation probed via controlled oxygen vacancy doping in epitaxial $BaSnO_3$, APL Mater. **5**, 056102 (2017).

[51] C. A. Niedermeier, S. Rhode, K. Ide, H. Hiramatsu, H. Hosono, T. Kamiya, and M. A. Moram, Electron effective mass and mobility limits in degenerate perovskite stannate $BaSnO_3$, Phys. Rev. B **95**, 161202(R) (2017).

[52] Y. Ozaki, D. Kan, and Y. Shimakawa, Influence of cation off-stoichiometry on structural and transport properties of (Ba, La)SnO_3 epitaxial thin films grown by pulsed laser deposition, J. Appl. Phys. **121**, 215304 (2017).

[53] A. Prakash, P. Xu, X. Wu, G. Haugstad, X. Wang, and B. Jalan, Adsorption-controlled growth and the influence of stoichiometry on electronic transport in hybrid molecular beam epitaxy-grown $BaSnO_3$ films, J. Mater. Chem. C **5**, 5730 (2017).

[54] K. Ganguly, P. Ambwani, P. Xu, J. S. Jeong, K. A. Mkhoyan, C. Leighton, and B. Jalan, Structure and transport in high pressure oxygen sputter-deposited $BaSnO_{3-\delta}$, APL Mater. **3**, 062509 (2015).

[55] D. O. Scanlon, Defect engineering of $BaSnO_3$ for high-performance transparent conducting oxide applications, Phys. Rev. B **87**, 161201(R) (2013).

[56] U. Kim, C. Park, T. Ha, R. Kim, H. S. Mun, H. M. Kim, H. J. Kim, T. H. Kim, N. Kim, J. Yu, K. H. Kim, J. H. Kim, and K. Char, Dopant-site-dependent scattering by dislocations in epitaxial films of perovskite semiconductor $BaSnO_3$, APL Mater. **2**, 056107 (2014).

[57] J. Herrero-Martín, J. L. García-Muñoz, S. Valencia, C. Frontera, J. Blasco, A. Barón-González, G. Subías, R. Abrudan, F. Radu, E. Dudzik, and R. Feyerherm, Valence change of praseodymium in $Pr_{0.5}Ca_{0.5}CoO_3$ investigated by x-ray absorption spectroscopy, Phys. Rev. B **84**, 115131 (2011).

[58] F. Guillou, Q. Zhang, Z. Hu, C. Y. Kuo, Y. Y. Chin, H. J. Lin, C. T. Chen, A. Tanaka, L. H. Tjeng, and V. Hardy, Coupled valence and spin state transition in $(Pr_{0.7}Sm_{0.3})_{0.7}Ca_{0.3}Co_3$, Phys. Rev. B **87**, 115114 (2013).

[59] F. Guillou, Y. Bréard, and V. Hardy, Cobalt spin state above the valence and spin-state transition in $(Pr_{0.7}Sm_{0.3})_{0.7}Ca_{0.3}CoO_3$, Solid State Sci. **24**, 120 (2013).

[60] J. Padilla-Pantoja, J. Herrero-Martín, P. Gargiani, S. Manuel Valvidares, V. Cuartero, K. Kummer, O. Watson, N. B. Brookes, and J. Luis García-Muñoz, Stability of the cationic oxidation

states in $Pr_{0.50}Sr_{0.50}CoO_3$ across the magnetostructural transition by x-ray absorption spectroscopy, Inorg. Chem. **53**, 8854 (2014).

[61] M. Bickel, G. L. Goodman, L. Soderholm, and B. Kanellakopoulos, The magnetic susceptibility of Pr^{4+} in $BaPrO_3$: Evidence of long-range magnetic order, J. Solid State Chem. **76**, 178 (1988).

[62] M. N. Popova, S. A. Klimin, B. Z. Malkin, L. A. Kasatkina, G. Cao, and J. Crow, Crystal field and spectrum of Pr^{4+} in $BaPrO_3$, Phys. Lett. A **223**, 308 (1996).

[63] Y. Hinatsu and N. Edelstein, Electron paramagnetic resonance spectrum of Pr^{4+} in $BaCeO_3$, J. Solid State Chem. **112**, 53 (1994).

[64] Y. Hinatsu, Electron paramagnetic resonance spectra of Pr^{4+} in $BaCeO_3$, $BaZrO_3$, $BaSnO_3$, and their solid solutions, J. Solid State Chem. **122**, 384 (1996).

[65] K. Tezuka and Y. Hinatsu, Electron paramagnetic resonance study of Pr^{4+} ions doped in $BaHfO_3$ perovskite, J. Solid State Chem. **156**, 203 (2001).

[66] B. T. Thole, G. van der Laan, J. C. Fuggle, G. A. Sawatzky, R. C. Karnatak, and J. M. Esteva, $3d$ x-ray-absorption lines and the $3d^9 4f^{n+1}$ multiplets of the lanthanides, Phys. Rev. B **32**, 5107 (1985).

[67] J. B. Goedkoop, B. T. Thole, G. van der Laan, G. A. Sawatzky, F. M. F. de Groot, and J. C. Fuggle, Calculations of magnetic x-ray dichroism in the 3d absorption spectra of rare-earth compounds, Phys. Rev. B **37**, 2086 (1988).

[68] J. B. Goedkoop, X-ray dichroism of rare earth materials, Doctoral dissertation, Ketholieke Universiteit te Nijmegen, 1989.

[69] S. Sallis, D. O. Scanlon, S. C. Chae, N. F. Quackenbush, D. A. Fischer, J. C. Woicik, J.-H. Guo, S. W. Cheong, and L. F. J. Piper, La-doped $BaSnO_3$—Degenerate perovskite transparent conducting oxide: Evidence from synchrotron x-ray spectroscopy, Appl. Phys. Lett. **103**, 042105 (2013).

[70] S. A. Chambers, T. C. Kaspar, A. Prakash, G. Haugstad, and B. Jalan, Band alignment at epitaxial $BaSnO_3/SrTiO_3(001)$ and $BaSnO_3/LaAlO_3(001)$ heterojunctions, Appl. Phys. Lett. **108**, 152104 (2016).

[71] P. P. Balakrishnan, M. J. Veit, U. S. Alaan, M. T. Gray, and Y. Suzuki, Metallicity in $SrTiO_3$ substrates induced by pulsed laser deposition, APL Mater. **7**, 011102 (2019).

[72] E. Holmelund, J. Schou, S. Tougaard, and N. B. Larsen, Pure and Sn-doped ZnO films produced by pulsed laser deposition, Appl. Surf. Sci. **197-198**, 467 (2002).

[73] B. Hadjarab, M. Trari, and M. Kebir, Physical characterization of the semiconducting deficient perovskite $BaSnO_{3-\delta}$, Mater. Sci. Semi. Proc. **29**, 283 (2015).

[74] The theoretical prediction states that this type of defect occurs in oxygen-rich, metal-poor scenarios. This would be the opposite of our observations once again; for us, higher oxygen pressures lead to lower conductivities. As we discussed previously, it may be significant that the defect has a low formation energy, even if the exact conditions of the activation are at odds between our results and their theoretical predictions. Alternatively, growth in low oxygen pressures may not constitute "oxygen-poor" conditions due either to complications with PLD growth or a stringent definition of "rich" and "poor" in the theoretical study [55].